SCIENTIFIC ARTICLE

Corrective Osteotomy for Malunited Intra-Articular Fracture of the Distal Radius Using a Custom-Made Surgical Guide Based on Three-Dimensional Computer Simulation: Case Report

Kunihiro Oka, MD, Hisao Moritomo, MD, Akira Goto, MD, Kazuomi Sugamoto, MD, Hideki Yoshikawa, MD, Tsuyoshi Murase, MD

We report a case of malunited intra-articular fracture of the distal radius successfully treated with corrective osteotomy through an extra-articular approach using a custom-made surgical guide that was designed based on preoperative three-dimensional computer simulation. *(J Hand Surg 2008;33A:835–840. Copyright © 2008 by the American Society for Surgery of the Hand. All rights reserved.)*

Key words: Computer simulation, corrective osteotomy, malunited intra-articular fracture, surgical guide.

Malunited intra-articular fracture of the distal radius may cause pain, restrict the range of motion, and result in osteoarthritis of the wrist joint.[1–7] Recently, several investigators have reported different techniques of intra-articular corrective osteotomy for symptomatic intra-articular malunion.[8–11] However, even with these techniques, it is still difficult to perform an accurate osteotomy through the original fracture line on the articular surface and reduce the malunited fragment to the correct position to reconstruct a smooth joint surface.[11] An operative procedure involving arthrotomy has the inherent risk of postoperative joint contracture.[8] The malunited fragment, if completely dissected from the parent radius, can become necrotic.[9,10] Less-invasive arthroscopic procedures require considerable surgical skills to accomplish an appropriate intra-articular corrective osteotomy. On the other hand, the recent progress in computed tomography (CT) imaging and computer technology has enabled us to simulate an accurate three-dimensional (3-D) corrective osteotomy using CT bone models. Furthermore, the development of an intraoperative guiding system that uses a custom-made surgical template makes it possible to perform an operation as simulated before the actual operation in spinal surgery,[12–14] joint arthroplasty,[15] and dental implantation.[16,17]

Here, we report a case of malunited intra-articular fracture of the distal radius that was successfully treated through an extra-articular approach using a simulation guidance system that consists of an original 3-D computer program and a custom-made surgical guide, which was designed to reproduce a preoperative simulation during the actual surgery.

From the Department of Orthopaedic Surgery, Osaka University Graduate School of Medicine, Osaka, Japan.

Received for publication December 21, 2007; accepted in revised form February 8, 2008.

This work was supported in part by the Japan Science and Technology Agency.

Corresponding author: Tsuyoshi Murase, MD, Department of Orthopaedic Surgery, Osaka University Graduate School of Medicine, 2-2, Yamada-oka, Suita, Osaka 565-0871, Japan; e-mail: tmurase-osk@umin.ac.jp.

0363-5023/08/33A06-0005$34.00/0
doi:10.1016/j.jhsa.2008.02.008

CASE REPORT

A 32-year-old man sustained a volar Barton fracture of the left distal radius and was initially treated by open reduction and internal fixation with a volar plate. The fracture united and the plate was removed 5 months after the operation; however, the patient complained of wrist pain and restriction of wrist motion. He was subsequently referred to our institution.

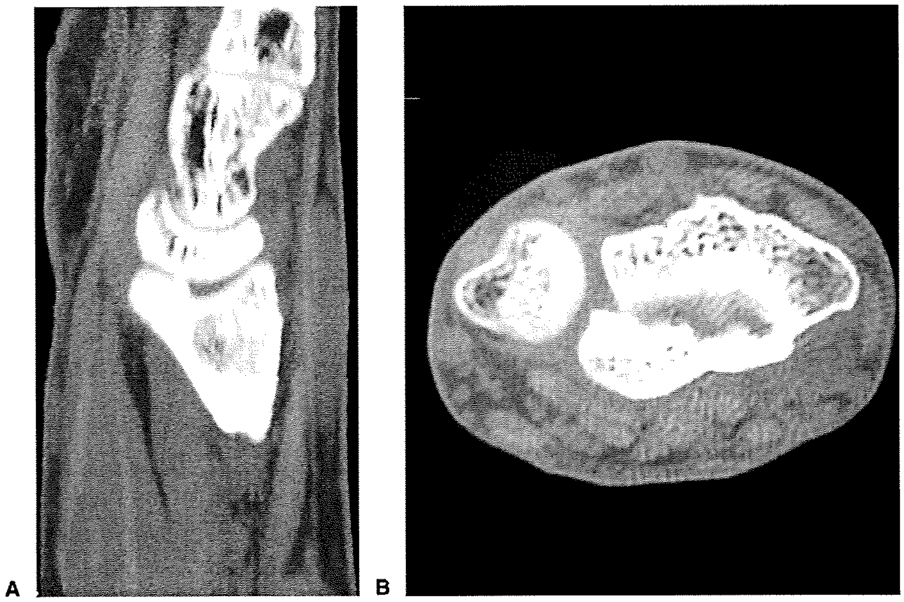

FIGURE 1: Computed tomography showed **A** a 3-mm step-off of the articular surface of the distal radius and **B** distal and ulnar migration of the volar fragment.

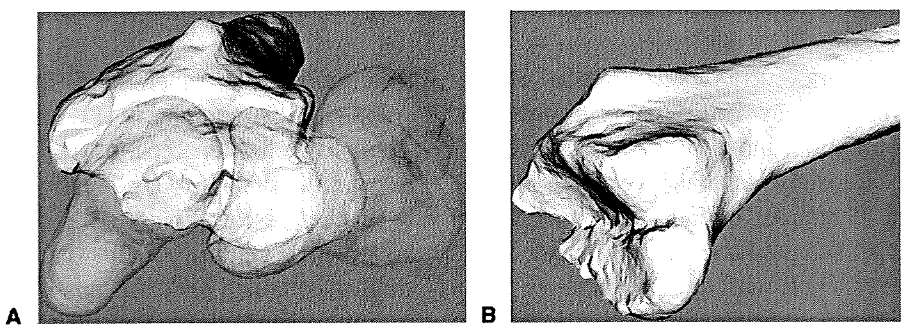

FIGURE 2: A, B A 3-D bone model of the radius indicates a malunion of the ulnovolar fragment of the distal radius.

On physical examination, wrist extension and flexion were restricted to 45° and 5°, respectively, with marked pain. Grip strength was 22 kg compared to 53 kg in the opposite hand. Radiographs revealed an irregular articular surface of the distal radius. CT showed a 3-mm articular step-off with distal migration of the fragment (Fig. 1).

Simulation

To plan corrective surgery for this intra-articular deformity of the distal radius, we attempted to simulate the 3-D correction of the deformity using computer models of the bones. First, the wrist was scanned by CT (scan time 0.5 s, slice thickness 0.625 mm, 10 mA, 120 kV; LightSpeed Ultra 16, General Electric, Waukesha, WI), and the digital data were entered in the computer. The contours of the radius, ulna, and proximal row of the carpal bones were semiautomatically segmented, and 3-D surface models were constructed based on the 3-D surface generation of the bone's cortex[18] using a VTK-based original computer program (Visualization Toolkit; Kitware Inc., Clifton Park, NY). Then, by deleting the bone marrow data, we obtained the complete surface models of the bones. The 3-D bone model of the radius showed a step-off at the articular surface of the distal radius with distal migration of the volar fragment (Fig. 2). In the computer simulation, the volar fragment was divided along the step-off and was reduced to the level of the original articular surface. The correction was completed by sliding the volar fragment 3 mm in the proximal direction (Fig. 3). To reproduce this simulation of intra-articular corrective osteotomy through an extra-articular approach, a customized surgical guide with multiple drilling holes to divide the malunited fragment was designed using commercially available software (Magics RP 10; Materialize, Leuven, Belgium) to exactly fit onto the volar surface of the distal

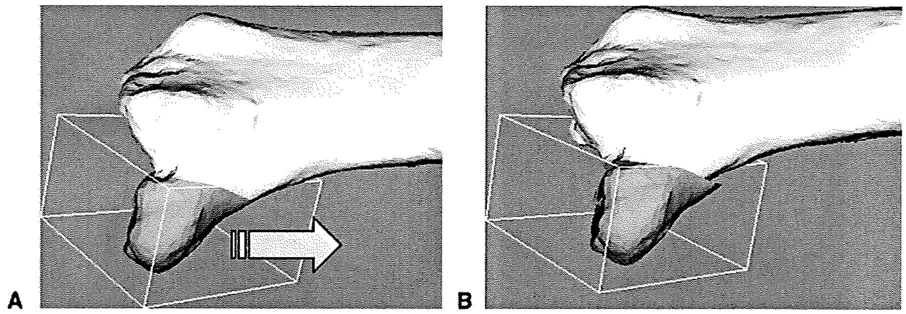

FIGURE 3: **A, B** Correction of the radius was accomplished by sliding the volar fragment 3 mm proximally.

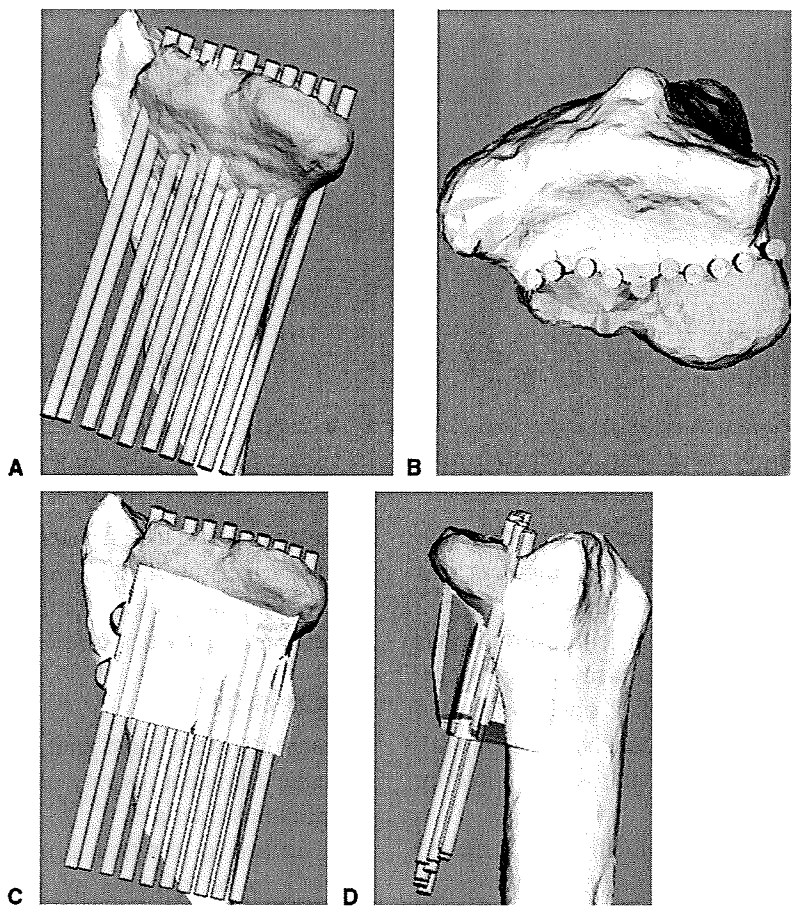

FIGURE 4: Computer planning of an intra-articular osteotomy. **A, B** Multiple wires (blue) were set along the deformity line to perform osteotomy. **C, D** A customized surgical guide (yellow), which fit on the bone surface and which was equipped with drill holes, was designed.

radius (Fig. 4). Then, the surgical guide was molded as a real plastic model with medical-grade resin in a rapid prototyping machine (Eden 250; Objet Geometries Ltd., Rehovot, Israel), which was accurate to within 30 μm. The guide was equipped with guide holes to set sleeves for K-wires. The diameter of the guide hole for a stainless drill sleeve, which had an internal diameter of 1.3 mm, was set at 3.0 mm. The surgical guide was sterilized with ethylene oxide (Fig. 5).

Surgical technique

The volar surface of the distal radius was exposed through a conventional volar approach, and the surgical guide was closely fit. K-wires (1.2 mm [0.047 in]) were passed through a drill sleeve while confirming penetration of the ends through the articular step-off under arthroscopic visualization (Fig. 6A, B). In total, 10 wires were placed, and an osteotomy was accomplished using a chisel along the borings (Fig. 6C). The fragment

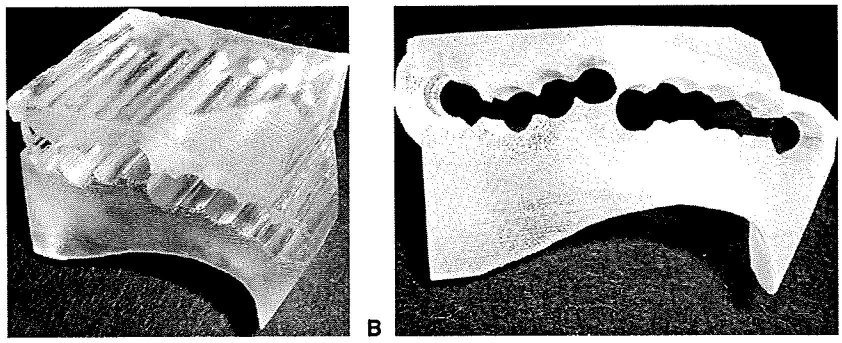

FIGURE 5: A, B The surgical guide was embodied as a real plastic model.

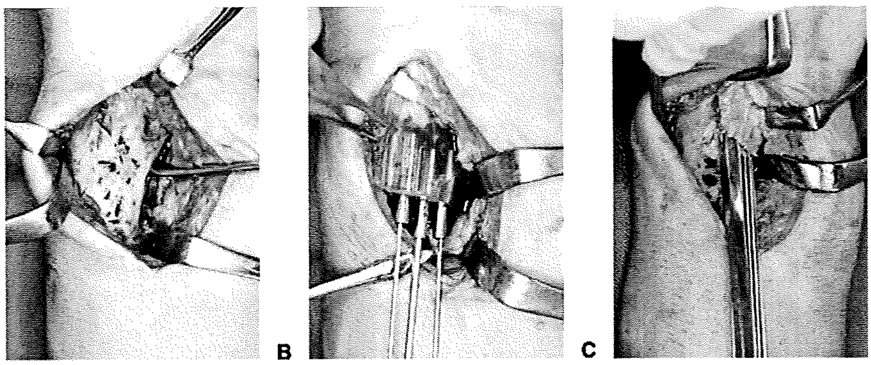

FIGURE 6: A The volar surface of the distal radius was exposed. **B** The surgical guide was fit, and K-wires were passed through drill sleeves under arthroscopic visualization. **C** The bone was divided using a chisel along the borings.

was completely separated from the radius with the volar radiocarpal ligaments attached to it. The fragment was moved proximally 3 mm and fixed temporally with 2 K-wires. After the reduction of the articular surface was confirmed with arthroscopy and an x-ray image intensifier, the fragment was fixed with 2 double-threaded screws (DTJ screw; Meira Co., Ltd., Nagoya, Japan), which have been shown to provide strong holding power for small bone fragments.[19]

Complete reduction of the step-off was achieved without arthrotomy, and a postoperative radiograph clearly showed that the incongruity of the radiocarpal joint was corrected. Cast immobilization was maintained for 3 weeks postoperatively. The patient was able to actively exercise the wrist and forearm, under the supervision of a physiotherapist, because good fixation between the fragment and the radius was achieved and wrist contracture after the intra-articular osteotomy was prevented. Three months after surgery, bone union had been achieved, the range of motion had improved, and the pain had disappeared. At the final follow-up 3 years after surgery, the congruity of the radiocarpal joint was preserved on radiographs (Fig. 7), and a smooth radial articular surface was observed on CT scans (Fig. 8). Wrist extension and flexion improved to 80° and 70°, respectively, and the grip strength increased from 22 kg preoperatively to 45 kg postoperatively. Furthermore, the patient no longer complained of any functional limitation in activities of daily living.

DISCUSSION

Incongruity of the wrist joint because of displaced intra-articular fragments is one of the major concerns after distal radius fractures.[2,4,7,20] Failure to reduce the articular surface to less than 2 mm of the step-off is considered to be a cause of posttraumatic osteoarthritis,[4,7,8,10] for which partial or total wrist arthrodesis has often been indicated.[21–25] Few studies have reported corrective osteotomies for intra-articular malunions of the distal radius, with and without arthroscopic assistance; however, these procedures are still associated with problems.[4,8,10,11] It is not always possible to adequately evaluate the complex 3-D intra-articular malunion with plain radiographs and intermittent slices of CT images. Consequently, the first problem that a surgeon encounters is planning an appropriate corrective surgery. In the actual surgery, it is not easy to perform an accurate osteotomy through a malunited fracture line from a limited field of view. Arthrotomy is usually performed from the dorsal side of the wrist joint to

FIGURE 7: Anatomic correction and congruity of the radiocarpal joint was obtained after surgery. **A** Anteroposterior and **B** lateral radiographs 3 years and 4 months after surgery are shown.

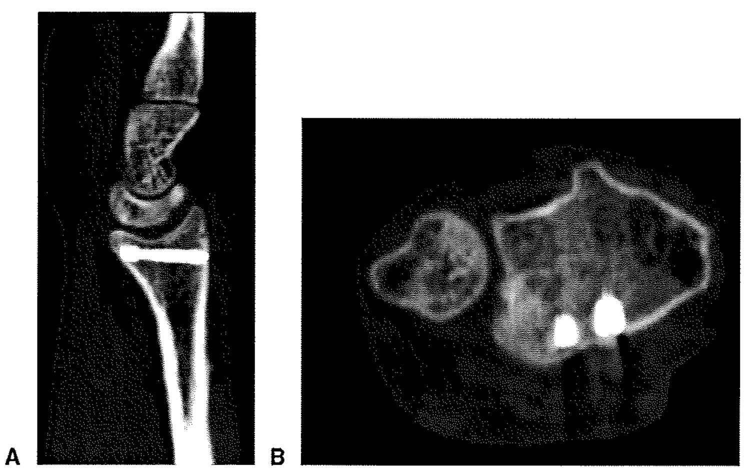

FIGURE 8: A, B Computed tomography shows congruity of the radiocarpal joint and complete obliteration of the step-off.

preserve the volar radiocarpal ligaments, which are the main stabilizers of the radiocarpal and midcarpal joints. Therefore, a malunited fragment located at the volar articular surface is difficult to operate on. Concerning postoperative wrist function, an open procedure of the wrist joint might lead to restricted range of joint motion due to fibrosis. Arthroscopic surgery is a less invasive alternative for managing intra-articular pathology. However, it is technically demanding to insert a targeting device into the tight volar joint space of the wrist, place it exactly on the fracture line, and perform an appropriate osteotomy under arthroscopic visualization.

We tried to perform an accurate intra-articular corrective osteotomy using 3-D computer simulation and a custom-made surgical guide. The advantage of the computer simulation is its ability to devise an accurate operative plan with CT bone models. The customized surgical guide enabled us to realize the preoperative simulation of intra-articular corrective osteotomy through an extra-articular approach during the actual surgery. A CT-based, custom-made surgical guide has been reported to be used in spinal surgery techniques such as insertion of pedicle screws,[12–14] total joint arthroplasty for bone cutting,[15] and innominate osteotomy,[26] and this procedure has been confirmed as a practical method for implementation of computerized planning. Custom-made drill guides have also been commercially produced for performing dental implants.[17,18] We modified this technique for performing a corrective osteotomy of a malunited intra-articular fracture. By making multiple drill holes on the guide, we were able to perform an accurate osteotomy through the malunited fracture line on the articular surface through an extra-articular approach, just as preoperatively simulated. After the osteotomy was performed, the reduction could be completed simply by sliding the fragment proximally. Although arthroscopy was performed, it was only used to confirm that each step of the surgical procedure was done correctly.

The computer program described here is currently available only at our institution. Approximately 2 hours was required to complete the preoperative simulation, and the CT scanning and stereolithography modeling cost about $180 and $360, respectively. We believe that these shortcomings can be overcome with the advancement of technology and could well be offset by the above-mentioned advantages. This initial account of an intra-articular corrective osteotomy assisted by computer simulation and a custom-made surgical guide indicates that accurate and reliable anatomic reduction and an excellent clinical outcome can be achieved with this technique. We believe that our technique of computer simulation guidance is useful in planning and performing intra-articular corrective surgery through an extra-articular approach and hope that it will provide a novel treatment option for malunited intra-articular distal radius fractures.

REFERENCES

1. Fernandez DL, Geissler WB. Treatment of displaced articular fractures of the radius. J Hand Surg 1991;16A:375–384.
2. Trumble TE, Schmitt SR, Vedder NB. Factors affecting functional outcome of displaced intra-articular distal radius fractures. J Hand Surg 1994;19A:325–340.
3. Axelrod T, Paley D, Green J, McMurtry RY. Limited open reduction of the lunate facet in comminuted intra-articular fractures of the distal radius. J Hand Surg 1988;13A:372–377.
4. Bradway JK, Amadio PC, Cooney WP. Open reduction and internal fixation of displaced, comminuted intra-articular fractures of the distal end of the radius. J Bone Joint Surg 1989;71A:839–847.
5. Melone CP Jr. Open treatment for displaced articular fractures of the distal radius. Clin Orthop Relat Res 1986;202:103–111.
6. Szabo RM, Weber SC. Comminuted intraarticular fractures of the distal radius. Clin Orthop Relat Res 1988;230:39–48.
7. Knirk JL, Jupiter JB. Intra-articular fractures of the distal end of the radius in young adults. J Bone Joint Surg 1986;68A:647–659.
8. Gobel F, Vardakas DG, Riano F, Vogt MT, Sarris I, Sotereanos DG. Arthroscopically assisted intra-articular corrective osteotomy of a malunion of the distal radius. Am J Orthop 2004;33:275–277.
9. del Pinal F, Garcia-Bernal FJ, Delgado J, Sanmartin M, Regalado J, Cerezal L. Correction of malunited intra-articular distal radius fractures with an inside-out osteotomy technique. J Hand Surg 2006; 31A:1029–1034.
10. Ring D, Prommersberger KJ, Gonzalez del Pino J, Capomassi M, Slullitel M, Jupiter JB. Corrective osteotomy for intra-articular malunion of the distal part of the radius. J Bone Joint Surg 2005;87A:1503–1509.
11. Marx RG, Axelrod TS. Intraarticular osteotomy of distal radial malunions. Clin Orthop Relat Res 1996;327:152–157.
12. Goffin J, Van Brussel K, Martens K, Vander Sloten J, Van Audekercke R, Smet MH. Three-dimensional computed tomography-based, personalized drill guide for posterior cervical stabilization at C1-C2. Spine 2001;26:1343–1347.
13. Birnbaum K, Schkommodau E, Decker N, Prescher A, Klapper U, Radermacher K. Computer-assisted orthopedic surgery with individual templates and comparison to conventional operation method. Spine 2001;26:365–370.
14. Brown GA, Firoozbakhsh K, DeCoster TA, Reyna JR Jr, Moneim M. Rapid prototyping: the future of trauma surgery? J Bone Joint Surg 2003;85A(Suppl 4): 49–55.
15. Hafez MA, Chelule KL, Seedhom BB, Sherman KP. Computer-assisted total knee arthroplasty using patient-specific templating. Clin Orthop Relat Res 2006;444:184–192.
16. Garg AK. Surgical templates in implant dentistry. Dent Implantol Update 2006;17:41–44.
17. Sarment DP, Al-Shammari K, Kazor CE. Stereolithographic surgical templates for placement of dental implants in complex cases. Int J Periodontics Restorative Dent 2003;23:287–295.
18. Lorensen WE, Cline HE. Marching cubes: a high resolution 3D surface construction algorithm. Comput Graph 1987;21:163–169.
19. Tanaka J, Yanagida H, Oomukai T, Okuno T. A newly developed double thread screw for carpal scaphoid fracture. J Jpn Soc Surg Hand 2002;19:643–647.
20. Catalano LW III, Cole RJ, Gelberman RH, Evanoff BA, Gilula LA, Borrelli J Jr. Displaced intra-articular fractures of the distal aspect of the radius. Long-term results in young adults after open reduction and internal fixation. J Bone Joint Surg 1997;79A:1290–1302.
21. Rayan GM. Wrist arthrodesis. J Hand Surg 1986;11A:356–364.
22. Weiss AP, Hastings H II. Wrist arthrodesis for traumatic conditions: a study of plate and local bone graft application. J Hand Surg 1995;20A:50–56.
23. Richterman I, Weiss AP. Wrist fusion. Hand Clin 1997;13:681–687.
24. Nagy L. Salvage of post-traumatic arthritis following distal radius fracture. Hand Clin 2005;21:489–498.
25. Yajima H, Kobata Y, Shigematsu K, Kawamura K, Takakura Y. Radiocarpal arthrodesis for osteoarthritis following fractures of the distal radius. Hand Surg 2004;9:203–209.
26. Radermacher K, Portheine F, Anton M, Zimolong A, Kaspers G, Rau G, et al. Computer assisted orthopaedic surgery with image based individual templates. Clin Orthop Relat Res 1998;354:28–38.

THE INTERNATIONAL JOURNAL OF MEDICAL ROBOTICS AND COMPUTER ASSISTED SURGERY
Int J Med Robotics Comput Assist Surg 2009; **5**: 164–169.
Published online 26 February 2009 in Wiley InterScience (www.interscience.wiley.com). **DOI:** 10.1002/rcs.243

ORIGINAL ARTICLE

Tailor-made surgical guide based on rapid prototyping technique for cup insertion in total hip arthroplasty

Takehito Hananouchi[1]*
Masanobu Saito[2]
Tsuyoshi Koyama[2]
Keisuke Hagio[2]
Tsuyoshi Murase[1]
Nobuhiko Sugano[3]
Hideki Yoshikawa[1]

[1]*Department of Orthopaedic Surgery, Osaka University Graduate School of Medicine, Osaka, Japan*

[2]*Department of Orthopaedic Surgery, Osaka Minami Medical Centre, Osaka, Japan*

[3]*Department of Orthopaedic Medical Engineering, Osaka University Graduate School of Medicine, Osaka, Japan*

*Correspondence to:
Takehito Hananouchi, 2-2 Yamadaoka, Suita 565-0871, Osaka, Japan.
E-mail: hana-osaka@umin.net

Accepted: 31 December 2008

Abstract

Background A surgical guide made by the rapid prototyping (RP) technique for cup insertion in total hip arthroplasty might be useful to avoid malalignment of the cup, which indicates postoperative complications.

Methods To address this research question, we applied a RP-based guide to 24 patients with their CT images. We designed it to fit onto the acetabular edge and to insert a Kirschner wire (K-wire) which indicated a planned cup direction. We intraoperatively placed it on the acetabular edge, inserted the K-wire through the guide on the superior acetabulum and implanted the cup while observing the alignment of the K-wire. We also recorded the additional time needed to use the guide.

Results The mean cup accuracy between planned and postoperative alignments was 2.8° (SD = 2.1°) for abduction and 3.7° (SD = 2.7°) for anteversion. The mean additional time was 3.5 (range 2–6) min.

Conclusion We can use this guide with acceptable accuracy and without consuming an excessive amount of time. Copyright © 2009 John Wiley & Sons, Ltd.

Keywords surgical guide; total hip arthroplasty; rapid prototyping technique; tailor-made

Introduction

In total hip arthroplasty (THA), fixation of the acetabular component (cup) requires optimal alignment, which is defined as a 'safe zone' by one author (1), in order to reduce postoperative complications, such as cup–neck impingement and hip dislocation. The zone is an abduction angle of 40 ± 10° and an anteversion angle of 15 ± 10°. With this range the dislocation rate was 1.5% and outside this range it was 6.1%. Because 22–71% of cases with the conventional manual procedure are achieved within the safe zone (2–5), some computer navigation systems with optical sensors have been used to reduce angle variations of the cup (4–7). However, this kind of system has a high cost per arthroplasty case (an additional $600–2000 for navigation) (8) and involves intraoperatively time-consuming procedures (an additional 15–46 min of operating time compared with conventional procedures) (8,9).

Another computer-assisted surgery technique that involves few time-consuming intraoperative procedures is the use of a tailor-made surgical guide, made using the rapid prototyping (RP) technique, which has been reported for various orthopaedic procedures, such as pelvic osteotomy (10), fixation for acetabular fracture (11), spinal instrumentation (10,12), knee arthroplasty (13) and corrective osteotomy of the upper extremity (14,15), as well as for dental implants (16,17). The surgical guide has a base part to fit on the surgical bone intraoperatively, and a guide part to achieve optimal alignment or position of the surgical instruments on the basis of preoperative computed tomography (CT) images of the relevant bone. Although there is some concern about taking CT images in this technique, some recent papers have reported an improvement to reduce the radiation dose (18,19).

Since the use of the surgical guide for cup insertion has not been reported previously, we applied the surgical guide to dry cadaveric pelvic bones (20). The surgical guide was designed to fit onto intact acetabular edges with the insertion of a Kirschner wire (K-wire) indicating a favourable cup direction. We showed in *the vitro* study that the mean error for the placement of the surgical guide was within 1° [abduction; 0.8° (range 0.2–2.3°, SD 0.8°); anteversion, 0.5° (range 0–2.0°, SD 0.6°)].

The purpose of the current study was to investigate whether the tailor-made surgical guide for cup insertion was useful in real clinical cases.

Materials and Methods

We examined the usefulness of the surgical guide for cup insertion in terms of accuracy of cup insertion and the time required for use of the surgical guide during the operation. The surgical guide for cup alignment was designed preoperatively on the computer using CT images of the patient's pelvis, and then the surgical guide was manufactured using the RP technique. The surgical guide was used during cup insertion in 24 patients. Patient mean age was 65.8 (range 52–87) years; there were two males and 22 females. The preoperative diagnosis was osteoarthritis in 17 patients, osteonecrosis of the femoral head in four patients and rheumatoid arthritis in three patients. This study was approved by the institutional review board, and all patients gave their written informed consent.

Preoperative CT images of the whole pelvis were obtained with a 2.5 mm slice thickness, slice pitch 3 mm (0.15 : 1) and pixel spacing 0.781 mm (Light Speed Plus, GE Medical Systems, Milwaukee, WI, USA). The images were transferred to computer software (3D template, Japan Medical Materials, Osaka, Japan) for 3D planning of the cup. In the software, we acquired any multi-plannar (coronal, sagittal and axial) views with a changing orthogonal coordinate system and any digitally reconstructed plain radiographs (DRR) on each view. The DRR was a synthetic X-ray (21) on the basis of the CT images (Figure 1). To make the pelvic coordinate system, we referenced the supine position of the patients when taking CT images (6,22). With this reference, we could determine the coronal plane corresponding to the plane of the CT table. Then, we defined a line joining the ischial tuberosities as the horizontal axis, with a DRR of anteroposterior direction on the coronal view (Figure 2a). In order to match between preoperative and postoperative pelvic orientations, we recorded the pelvic tilt with another DRR of lateral direction on the sagittal view (Figure 2b) (22) and the angle between the line joining the anterior superior iliac spines and the horizontal line in the axial view (Figure 2c). Abduction of the cup was planned to be 40° using the radiographic definition (23). Anteversion of the cup was planned with a range of 15–20° using the radiographic definition, because acetabular bony coverage and degree of femoral neck anteversion were considered. These angles were defined as the preoperative cup orientation. The matrix data of the cup orientation were recorded for the following process.

The CT images also were transferred to image processing software (Virtual Place-M; Medical Imaging Laboratory, Tokyo, Japan) to reconstruct a polygonal three-dimensional (3D) pelvic model using the marching cubes method (24). The surgical guide was designed by Visualization Toolkit (VTK) libraries (Kitware Inc., Clifton Park, NY, USA). After transferring the pelvic model, the

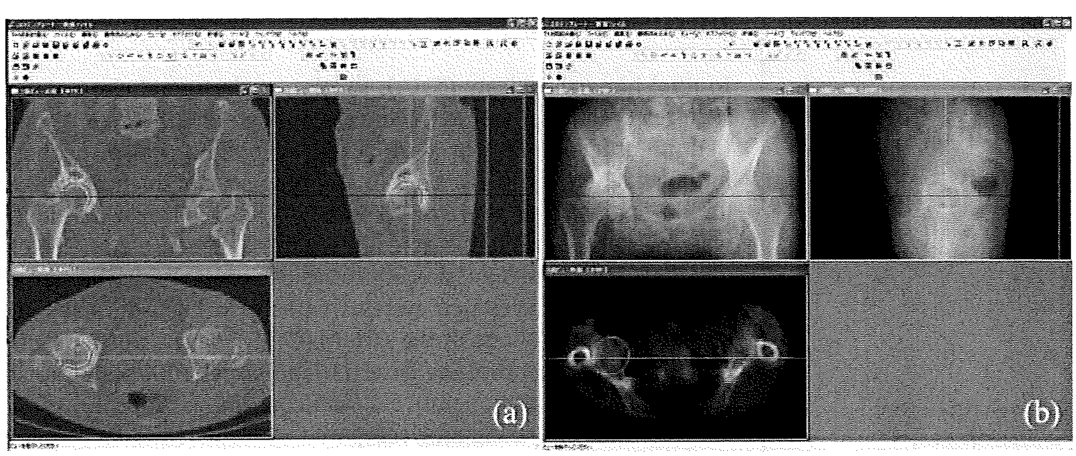

Figure 1. 3D planning of the cup. (a) multi-planar (coronal, sagittal and axial) views of CT images. (b) Digitally reconstructed radiographs on the basis of the CT images. We can acquire these with any orthogonal coordinate system

DOI: 10.1002/rcs

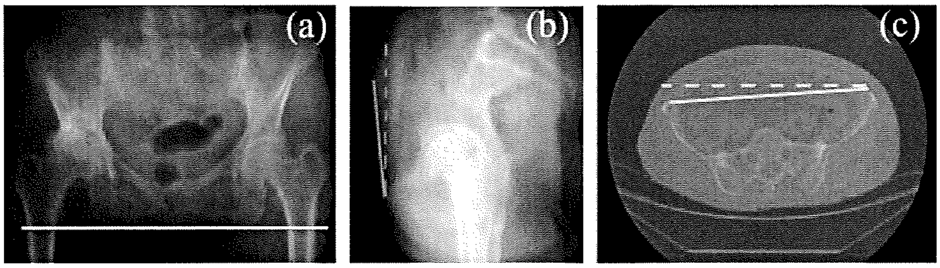

Figure 2. Pelvic coordinate system. (a) The coronal plane corresponded with the plane of the CT table. The line joining the the ischial tuberosities is defined as the horizontal axis (white line). To match between preoperative and postoperative pelvic orientations, the pelvic tilt (b) is the angle between the line of the anatomical plane of the pelvis (solid grey line), through the bilateral superior anterior iliac spines and the superior margin of the pubic symphysis and the vertical line (dotted grey line) on the sagittal view is recorded. The angle (c) between the line (solid white line) joining the bilateral superior iliac spines and the horizontal line (dotted white line) is also recorded

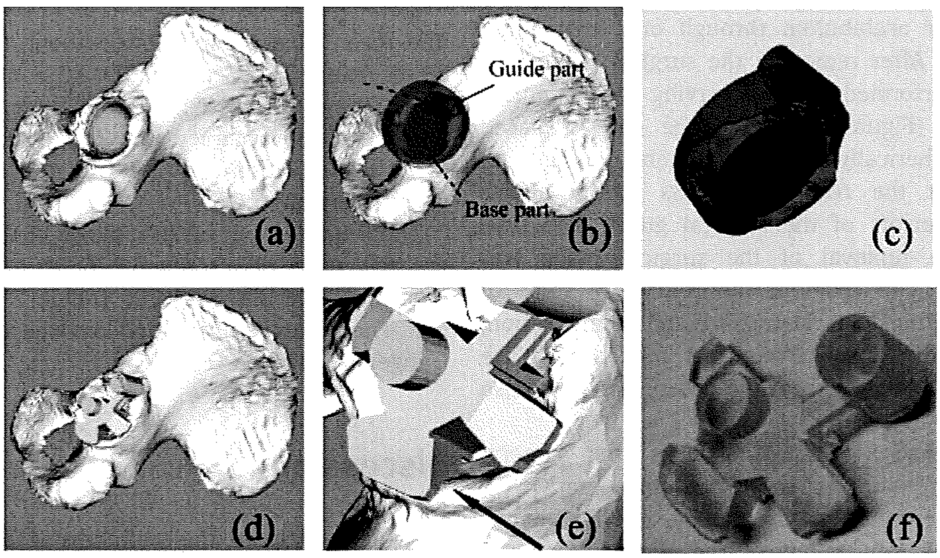

Figure 3. The making of the tailor-made surgical guide. (a) A 3D view of the cup and the pelvic model. (b) Premodel of the surgical guide, which consists of a guide (solid arrow) and base parts (dotted arrow). A broken line shows the alignment of the preoperatively planned cup. (c) Back of the premodel of the surgical guide (when looking from the acetabulum) has an imprint of the acetabular edge after Boolean subtraction. (d) Final model of the surgical guide is made by shaping itself. (e) Some parts used to confirm adaptation between the surgical guide and the acetabular edge are made by shaping of the surgical guide (an arrow indicates one of these confirmation parts). (f) Manufacture of the surgical guide using the RP technique

3D cup model was placed in the acetabulum on the basis of the matrix data (Figure 3a). By the placement of the cup, we could determine some intact parts of the acetabular edge, e.g. inferior parts around the transverse ligament (Figure 3a). The intact parts were used for shaping the surgical guide in the following steps. We designed the premodel of the surgical guide, which consisted of a base and guide parts (Figure 3b: solid arrow, guide part; dotted arrow, base part). The base part, which was a cylindrical object, was placed overlapping the acetabular edge. The guide part was another cylindrical bore and was designed to parallel the direction of the planned cup with its matrix data. The guide part also had cylindrical foramina in order to insert a 2 mm diameter K-wire on the superior acetabulum intraoperatively.

The pelvic model and the premodel of the surgical guide were exported in stereolithography (STL) format to Magics 11 (Materialise NV, Leuven, Belgium) software for spatial image processing to design the surgical guide. The guide part was combined with the base part. The base part was modified by spatially subtracting a part of the acetabular edge from itself, which is known as Boolean subtraction. This modification provided an imprint of the part of the acetabular edge in the base part (Figure 3c). Furthermore, the modified base part was shaped by removing itself partly to fit on only the intact acetabular edges, which were detected by placing the cup on the acetabulum (Figure 3d). Some confirmation points to investigate adaptation between the surgical guide and the acetabular edge intraoperatively were also made consequently by the shaping of the modified base part (Figure 3e; black arrow indicate one of the confirmation parts). The surgical guide was then manufactured with photosensitive medical-grade resin, using an RP machine (Eden 250; Objet Geometries Ltd, Rehovot, Israel; Figure 3f).

The surgical guide was used after femoral head resection, acetabular exposure, and acetabular reaming

DOI: 10.1002/rcs

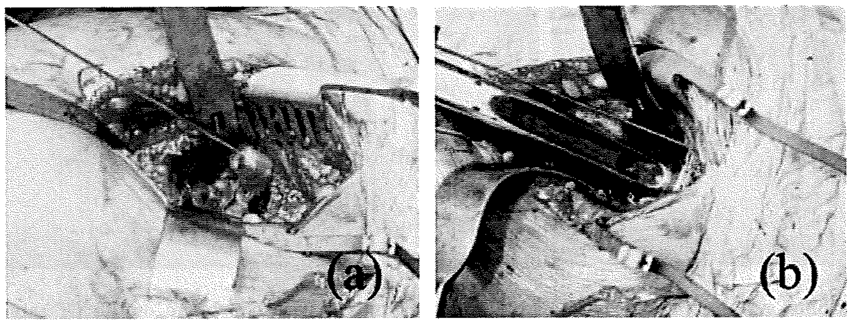

Figure 4. Cinical use of the tailor-made surgical guide during cup insertion of total hip arthroplasty. (a) Placement of the surgical guide and insertion of the K-wire through the guide part. (b) Cup fixation while observing the alignment of the K-wire

during THA. The surgical guide was placed on the periacetabulum (Figure 4a), and the K-wire was inserted on the superior acetabulum through one foramen of the guide part. After removing the surgical guide, cup fixation was performed while observing the alignment of the K-wire (Figure 4b). Since the cup is placed to the hemispherically reamed acetabulum, it was considered that the reaming process hardly affects the alignment errors of the surgical guide. The time from set-up to removal of the surgical guide was recorded. After cup fixation, the remaining steps of the THA, including femoral rasping and stem fixation, were performed using conventional procedures. The operative time and intraoperative blood loss were also recorded.

All patients had a CT scan 3 weeks after surgery. The pelvic coordinate system of the postoperative CT images was determined by the method described above (Figure 2a). The adjustment of the preoperative and postoperative pelvic orientations was performed using information of the preoperative pelvic tilt (Figure 2b) and the angle between the line joining the anterior superior iliac spines and the horizontal line (Figure 2c). The postoperative orientation of the cup was measured after the adjustment. The reproducibility of the measurement of the postoperative orientation of the cup, including in the adjustment between the preoperative and postoperative pelvic orientations, was investigated using the following two parameters, which were used in a previous report (25). Intra-individual (from two measurements separated by a 3-week interval) and inter-individual (by one surgeon and one technical assistant) reliabilities, using Pearson correlation coefficient, and intra- and inter-individual angle differences (absolute angle difference between two measurements) were evaluated. The intra- and inter-individual reliabilities were 0.91 and 0.92 for abduction and 0.94 and 0.88 for anteversion. The intra- and inter-individual angle differences were 1.6° (SD 1.2°) and 1.1° (SD 0.8°) for abduction, and 1.7° (SD 1.3°) and 1.7° (SD 0.9°) for anteversion. 'Cup accuracy', which was defined as the absolute difference between the preoperative cup orientation and the postoperative cup orientation, was measured in all patients.

Results

The mean postoperative orientations of the cup were 38.6° (range 34.0–43.1°; SD 2.7°) of abduction and 17.4° (range 6.3–27.2°; SD 5.6°) degrees of anteversion. The mean cup accuracy was 2.8° (range 0.4–7.7°; SD 2.1°) for abduction and 3.7° (range 0.1–9.3°; SD 2.7°) for anteversion.

The time from set-up to removal of the surgical guide was an average of 3.5 (range 2–6; SD 1.4) min; the mean total operative time was 106 (range 79–169; SD 23.7) min. The intraoperative blood loss was an average of 655 (range 190–1768; SD 330) ml.

Discussion

In the current study, the usefulness of the surgical guide, made using the rapid prototyping technique, to avoid malalignment of the cup was investigated. Although the surgical guide was used in only 24 patients, we consider that the surgical guide was useful in the clinical setting.

It appears that the cup accuracy using the surgical guide was acceptable. Although the mean accuracy of the placement of the surgical guide was <1° in our previous study using dry pelvic bones (20), we assumed that additional errors would occur in the current study with clinical cases. Of these errors, some intrinsic and extrinsic errors are considered (26). In the intrinsic errors, segmentation error was not significant because a previous study reported that the segmentation error was 0.2–0.5 mm with similar CT protocols (with a slice thickness of 4 mm and a pixel spacing of 0.71 mm) (27). The slice thickness (2.5 mm) of the CT images in the current study might increase the intrinsic errors because the slice thickness in our previous study was 1 mm (20). An error from the manufacture of the surgical guide was not significant because the accuracy of printing was 30 µm with high-speed mode and the overall accuracy was 0.1–0.2 mm, according to the brochure or the website of the company which provides the RP machine in the current study (www.objet.com). As to the extrinsic errors, we could address carefully the remove of soft tissues around the periacetabulum, which might affect

DOI: 10.1002/rcs

the accuracy of the placement of the surgical guide. An error during insertion of the K-wire and adjusting the cup alignment while observing the alignment of the K-wire was within 2°, according to our previous study (20). In addition, press-fit fixation of the cup affects final cup alignment (28). In this previous study on the undesirable effect of the press-fit procedure on the final alignment of the cup, the author showed that the mean absolute cup alignment deviations during implantation were 3.7° of abduction (range 0–9°; SD 2.8°) and 5.1° of anteversion (range 0–10°; SD 2.3°). Although many errors were considered as above, the cup accuracy was, on average, 2.8° for abduction and 3.7° degrees for anteversion. We believe that this cup accuracy achieved by the surgical guide was favourable compared with the following results of conventional and navigated THAs according to previous papers (2–7,29,30).

The mean absolute deviation from preoperative planned alignment of the cup was 4.1–6.3° (maximum 25°) for abduction and 5.2–13.0° (maximum 38°) for anteversion in conventional THAs, and 3.6–4.2 (maximum 15°) for abduction and 4.2–5.3° (maximum 18°) for anteversion in the navigated THAs (2–5,29). With regard to a range within 10° from the desired alignment of the cup, such as the safe zone, 22–71% of the cases with conventional THAs and 80–100% of the cases with the navigated THAs (2–6,30) achieved within the range. The all cup alignments in our study were within 10° from the preoperative planned alignments. Therefore, we consider that our results are more favourable than conventional THAs and comparable to navigated THAs.

We evaluated whether the surgical guide was useful in terms of operating time and blood loss. Although it has been reported that the additional operation time was 15–46 minutes compared with conventional procedures (8,9), the mean time for use of the surgical guide in the current study was about 3.5 min. We consider that this time was not clinically significant. Because the time for the surgical guide was short, the total operation time (average 106 min) and blood loss (average 655 ml) in our study were comparable to some of the previous studies with the conventional and navigated THAs which we evaluated regarding the accuracy of the cup (4,6,7,29,30). The mean total operation time and mean blood loss were 75–178 min and 399–751 ml, respectively, in previous studies with conventional THAs (4,6,7,29) and 83–177 minutes and 341–827 ml in previous studies with navigated THAs (4,6,7,29,30).

Use of the surgical guide maintained the conventional intraoperative procedure. After acetabular reaming, we just placed the surgical guide and inserted the K-wire through the surgical guide. Then, we performed the cup fixation while observing the alignment of the K-wire as the alignment guide for the planned cup. No additional skin incisions for intraoperative registration steps and monitoring space for a computer are needed.

The surgical guide has also some advantages. First, the surgeon can obtain information about cup alignment without looking away from the surgical field. Since most commercial surgical navigation systems display images on a computer monitor positioned adjacent to the surgical field, surgeons might have physical and/or mental difficulty in adjusting between real and computational spatial information, and there may be potential risk to the surgical field while acquiring navigation information on the monitor. We suggest that the procedures involved in using the surgical guide maintain safety, because the surgeon does not have to look away from the surgical field. Second, this surgical guide can be used in any hospital. One needs to only take CT images of the patient, manufacture the surgical guide and sterilize it before the operation. No additional personnel are needed in the operating theatre (10).

There are some drawbacks to the surgical guide. Radiation exposure from the CT scans is a concern. However, it might be justified by the benefits of the imaging information, such as thickness and coverage of the acetabulum and femoral anteversion for implantation in 3D planning. In addition, attempts have been made to develop low-dose radiation CT scans of the pelvis (19). According to a previous paper, the radiation dose for the pelvis with 1–1.5 mm slice thickness was 1.7 mSv, as opposed to 10 mSv for a traditional pelvic CT scan. By comparison, the radiation doses from plain AP and lateral pelvic radiographs are 0.7 and 0.8 mSv, respectively (19). Both preoperative planning and manufacturing of the surgical guide required 90–120 minutes each. Apart from the time for its manufacture, the time for preoperative planning might shorten if dedicated computer software were made for the surgical guide.

In conclusion, the tailor-made surgical guide using the RT technique is useful for cup insertion during total hip arthroplasty in the clinical setting. The mean absolute deviation from preoperative planned alignment of the cup was 2.8° (range 0.4–7.7°; SD 2.1°) for abduction and 3.7° (range 0.1–9.3°; SD 2.7°) for anteversion. All cup alignments were within 10° of the preoperative planned alignments. The intraoperative time for using the surgical guide was an average of 3.5 (range 2–6; SD 1.4) min. Further study is needed to investigate whether the surgical guide provides more accuracy of cup insertion than conventional procedures, without excessive increase of the total operation time and blood loss.

Acknowledgements

This work was supported by grants from the Japan Hip Research Foundation Inc. and Research Fellowship of the Japan Society for the Promotion of Science for Young Scientists. The authors would like to thank Mr Wataru Yamanashi for supporting the technical aspects for this study, Dr Kunihiro Oka and Mr Ryoji Nakao for set-up at the start of this study, Dr Takashi Nishii, Dr Takashi Sakai and Dr Masaki Takao in Osaka University Graduate School of Medicine, Dr Nobuo Nakamura, Dr Akihiro Kakimoto, Dr Daiki Iwana and Dr Makoto Kitada in Kyowakai Hospital for the preliminary study, Dr Kazuo Yonenobu, Dr Mariko Ohshima and Dr Kensuke Ikuta in Osaka Minami Medical Centre for supporting the operative work and Ms Maki Hananouchi for technical assistance.

References

1. Lewinnek GE, Lewis JL, Tarr R, *et al.* Dislocations after total hip replacement arthroplasties. *J Bone Joint Surg Am* 1978; **60**: 217–220.
2. Boosker BH, Verheyen CC, Horstmann WG, *et al.* Poor accuracy of free hand cup positioning during total hip arthroplasty. *Arch Orthop Trauma Surg* 2007; **127**: 375–379.
3. DiGioia AM, Jaramaz B, Plakseychuk AY, *et al.* Comparison of a mechanical acetabular alignment guide with computer placement of the socket. *J Arthroplasty* 2002; **17**: 359–364.
4. Kalteis T, Handel M, Bathis H, *et al.* Imageless navigation for insertion of the acetabular component in total hip arthroplasty: is it as accurate as Ct-based navigation? *J Bone Joint Surg Br* 2006; **88**(2): 163–167.
5. Parratte S, Argenson JN. Validation and usefulness of a computer-assisted cup-positioning system in total hip arthroplasty. A prospective, randomized, controlled study. *J Bone Joint Surg Am* 2007; **89**(3): 494–499.
6. Sugano N, Nishii T, Miki H, *et al.* Mid-term results of cementless total hip replacement using a ceramic-on-ceramic bearing with and without computer navigation. *J Bone Joint Surg Br* 2007; **89**(4): 455–460.
7. Murphy SB, Ecker TM, Tannast M. THA performed using conventional and navigated tissue-preserving techniques. *Clin Orthop Relat Res* 2006; **453**: 160–167.
8. Beringer DC, Patel JJ, Bozic KJ. An overview of economic issues in computer-assisted total joint arthroplasty. *Clin Orthop Relat Res* 2007; **463**: 26–30.
9. Widmer KH, Grützner PA. Joint replacement – total hip replacement with CT-based navigation. *Injury* 2004; **35**(suppl 1): SA84–89.
10. Radermacher K, Portheine F, Anton M, *et al.* Computer assisted orthopaedic surgery with image based individual templates. *Clin Orthop Relat Res* 1998; **354**: 28–38.
11. Brown GA, Milner B, Firoozbakhsh K. Application of computer-generated stereolithography and interpositioning template in acetabular fractures: a report of eight cases. *J Orthop Trauma* 2002; **16**(5): 347–352.
12. Birnbaum K, Schkommodau E, Decker N, *et al.* Computer-assisted orthopedic surgery with individual templates and comparison to conventional operation method. *Spine* 2001; **26**(4): 365–370.
13. Hafez MA, Chelule KL, Seedhom BB, *et al.* Computer-assisted total knee arthroplasty using patient-specific templating. *Clin Orthop Relat Res* 2006; **444**: 184–192.
14. Oka K, Moritomo H, Goto A, *et al.* Corrective osteotomy for malunited intra-articular fracture of the distal radius using a custom-made surgical guide based on three-dimensional computer simulation: case report. *J Hand Surg Am* 2008; **33**(6): 835–840.
15. Murase T, Oka K, Moritomo H, *et al.* Three-dimensional corrective osteotomy of malunited fractures of the upper extremity with use of a computer simulation system. *J Bone Joint Surg Am* 2008; **90**: 2375–2389.
16. Lal K, White GS, Morea DN, Wright RF. Use of stereolithographic templates for surgical and prosthodontic implant planning and placement. Part I. The concept. *J Prosthodont* 2006; **15**(1): 51–58.
17. d'Hauthuille C, Taha F, Devauchelle B, *et al.* Comparison of two computer-assisted surgery techniques to guide a mandibular distraction osteogenesis procedure. Technical note. *Int J Oral Maxillofac Surg* 2005; **34**(2): 197–201.
18. Henckel J, Richards R, Lozhkin K, *et al.* Very low-dose computed tomography for planning and outcome measurement in knee replacement. The imperial knee protocol. *J Bone Joint Surg Br* 2006; **88**(11): 1513–1518.
19. Dandachli W, Kannan V, Richards R, *et al.* Analysis of cover of the femoral head in normal and dysplastic hips. New CT-based technique. *J Bone Joint Surg Br* 2008; **90**(11): 1428–1434.
20. Hananouchi T, Nishii T, Yamanashi W, *et al.* Surgical guide for acetabular insertion using rapid prototyping technique – *in vitro* study. *Int J Computer Assisted Radiology and Surgery* 2008; **3**(suppl 1): S243–S244.
21. Hananouchi T, Sugano N, Nakamura N, *et al.* Preoperative templating of femoral components on plain X-rays. Rotational evaluation with synthetic X-rays on ORTHODOC. *Arth Orthop Trauma Surg* 2007; **127**: 381–385.
22. Nishihara S, Sugano N, Nishii T, *et al.* Measurements of pelvic flexion angle using three-dimensional computed tomography. *Clin Orthop Relat Res* 2003; **444**: 184–192.
23. Murray DW. The definition and measurement of acetabular orientation. *J Bone Joint Surg Br* 1993; **75**(2): 228–232.
24. Lorensen WB, Cline HE. Marching Cubes: A high resolution 3D surface construction algorithm. *Comput Graphics (ACM)* 1987; **21**(4): 163–169.
25. Kalteis T, Handel M, Herold T, *et al.* Position of the acetabular cup – accuracy of radiographic calculation compared to CT-based measurement. *Eur J Radiol* 2006; **58**(2): 294–300.
26. Ruppin J, Popovic A, Strauss M, *et al.* Evaluation of the accuracy of three different computer-aided surgery systems in dental implantology: optical tracking vs. stereolithographic splint systems. *Clin Oral Implants Res* 2008; **19**(7): 709–716.
27. Färber M, Ehrhardt J, Handels H. Automatic atlas-based contour extraction of anatomical structures in medical images. *Int Congr Ser* 2005; **1281**: 272–277.
28. DiGioia AM, Jaramaz B, Blackwell M, *et al.* The Otto Aufranc award. Image guided navigation system to measure intraoperatively acetabular implant alignment. *Clin Orthop Relat Res* 1998; **355**: 8–22.
29. Najarian BC, Kilgore JE, Markel DC. Evaluation of component positioning in primary total hip arthroplasty using an imageless navigation device compared with traditional methods. *J Arthroplasty* 2009; (in press).
30. Hananouchi T, Takao M, Nishii T, *et al.* Comparison of navigation accuracy in THA between the mini-anterior and -posterior approaches. *Int J Med Robotics Comput Assist Surg* 2009; (in press).

Int J Med Robotics Comput Assist Surg 2009; 5: 164–169.
DOI: 10.1002/rcs

SCIENTIFIC ARTICLE

Interosseous Membrane of the Forearm: An Anatomical Study of Ligament Attachment Locations

Kazuo Noda, MD, Akira Goto, MD, PhD, Tsuyoshi Murase, MD, PhD, Kazuomi Sugamoto, MD, PhD, Hideki Yoshikawa, MD, PhD, Hisao Moritomo, MD, PhD

Purpose The interosseous membrane (IOM) of the forearm is a stout ligamentous complex that reportedly comprises several ligamentous components. The purpose of this cadaveric study was to define all IOM ligaments and to clarify the precise attachment locations.

Methods Thirty forearms from 15 embalmed cadavers were used. After dissection, all IOM ligaments were identified, and attachments were measured from the tip of the radial styloid or the ulnar head. Attachment locations were represented as a percentage of total bone length from the distal end of the radius or ulna.

Results The IOM included 5 kinds of ligaments: central band, accessory band, distal oblique bundle, proximal oblique cord, and dorsal oblique accessory cord. The most distal and proximal ends of the radial origin of the central band were 53% and 64% of total radial length from the tip of the radial styloid, whereas those of the ulnar insertion were 29% and 44% of total ulnar length from the ulnar head. The center point of the radial origin and ulnar insertion of the accessory band were 37% and 23%, respectively. The center points of the ulnar origins and radial insertions were 15% and 10% for the distal oblique bundle; 80% and 79% for the proximal oblique cord; and 64% and 62% for the dorsal oblique accessory cord, respectively.

Conclusions The present study clarified precise attachment locations of all representative IOM ligaments. This information will be useful in planning proper graft placement in ligament reconstruction surgery and for future biomechanics research into the function of the IOM ligaments. *(J Hand Surg 2009;34A:415–422. © 2009 Published by Elsevier Inc. on behalf of the American Society for Surgery of the Hand.)*

Key words Anatomy, attachment location, forearm, interosseous membrane (IOM), ligament.

THE INTEROSSEOUS MEMBRANE (IOM) of the forearm is a stout ligamentous complex linking the radius to the ulna. The anatomy of this structure has been studied by various investigators.[1–7] The IOM reportedly consists of distal membranous, middle ligamentous, and proximal membranous portions. Each portion is also known to include several ligamentous components. The most representative component of the IOM is called the central band (CB),[1,2] the broadest and stoutest collection of fibers in the IOM, running obliquely from the proximal radial shaft to the distal ulnar shaft. Prior biomechanical studies[1–3,8–11] have revealed that the CB plays important roles in maintaining forearm functions, as the longitudinal stabilizer of the forearm, and as a load transmitter between the radius and ulna.

The other components of the IOM reportedly comprise the accessory band (AB),[2] which is located adjacent to the CB; the proximal oblique cord[4,5,12–15] on the anterior aspect of the forearm; and the dorsal oblique accessory cord[5] on the posterior side. Some confusion seems to exist with regard to the terminology because prior authors have often used their own terms to repre-

From the Department of Orthopaedic Surgery, Osaka University Graduate School of Medicine, Suita, Osaka, Japan.

Received for publication April 18, 2008; accepted in revised form October 27, 2008.

No benefits in any form have been received or will be received related directly or indirectly to the subject of this article.

Corresponding author: Hisao Moritomo, MD, PhD, Osaka University Graduate School of Medicine, 2-2 Yamadaoka, Suita, Osaka 565-0871, Japan; e-mail: moritomo@ort.med.osaka-u.ac.jp.

0363-5023/09/34A03-0006$36.00/0
doi:10.1016/j.jhsa.2008.10.025

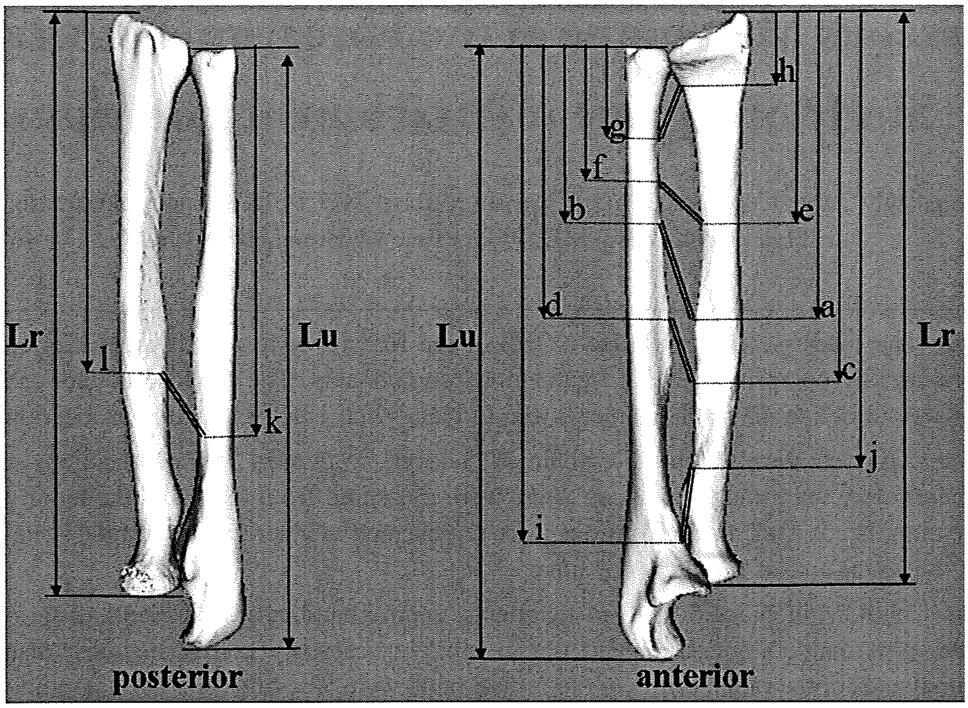

FIGURE 1: Measurement of attachment locations of IOM ligaments. Lr, radial length; Lu, ulnar length. a to l, lengths from the tip of the radial styloid for the radius or from the ulnar head for the ulna. Attachment locations are expressed as percentages of total bone length from the distal end (e.g., a/Lr ×100). a, b and c, d, distal and proximal ends of the central band; e, f, distal ligament of the accessory band; g, h, distal oblique bundle; i, j, proximal oblique cord; k, l, dorsal oblique accessory cord.

sent these structures, and the functions of these ligaments remain a mystery.

IOM researchers have documented the morphological characteristics of the IOM ligaments well, including measurements such as width,[1,2,4,5] thickness,[1,5,6] and insertion angle of the ligament into the radius and ulna.[2,7,16] The purpose of this study was to define all IOM ligaments and to clarify precise attachment locations.

MATERIALS AND METHODS

Thirty forearms from 15 embalmed cadavers (9 females, 6 males) were examined for the width, thickness, and attachment location of the IOM ligaments. Mean age at time of death was 85 years (range, 60–96 years). No apparent pathological lesions were identified in the forearms. The upper extremities were amputated at the middle of the upper arms. Specimens were carefully stripped of all soft tissues remaining on IOM structures and capsuloligamentous tissues around the wrists and elbows. The measurements were made with the forearm positioned in neutral rotation. The width and thickness of each IOM ligament was measured using calipers (accuracy, 0.05 mm; Mitutoyo, Kanagawa, Japan). We then identified the origins (proximal attachments) and insertions (distal attachments) of all ligaments. The locations of the attachments were measured from the tip of the radial styloid for the radius and from the ulnar head for the ulna (Fig. 1). For the CB, both the distal and proximal ends of attachment were measured because it had a broad attachment. For the other ligaments, only the center points of the attachments were measured because they had narrow attachments. A stainless steel ruler (accuracy, 0.15 mm; Shinwa Rules, Niigata, Japan) was used for location measurement. Attachment locations were expressed as percentages of the total bone length of the radius or the ulna from each distal end.

RESULTS

Middle ligamentous complex

The middle portion of the IOM (the middle ligamentous complex) was a complex of ligaments that were quadrilateral in shape and were located within the interosseous space. The middle ligamentous complex was further divided into 2 ligamentous components, the CB and the AB.

Central band: The widest and thickest ligament was the CB, forming part of the middle ligamentous complex (Figs. 2–5). The CB originated from the interosseous

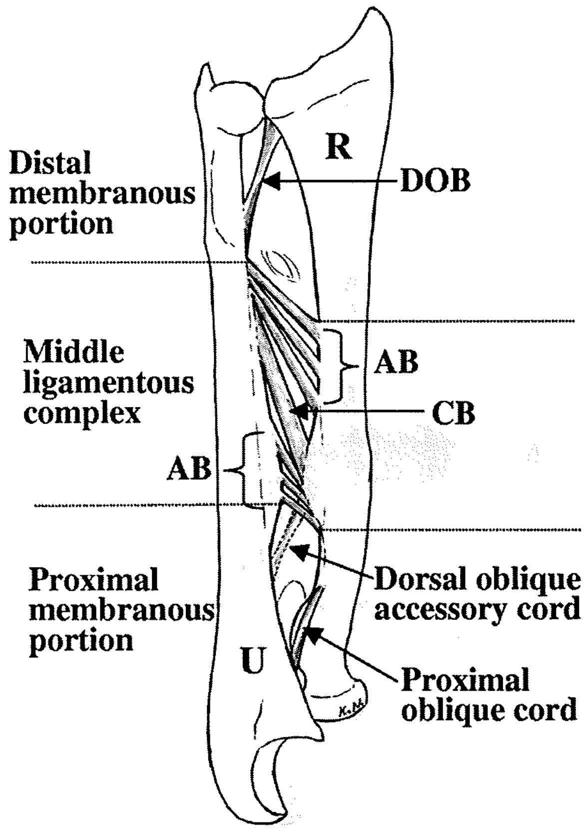

FIGURE 2: Schematic structure of the IOM. Right forearm viewed from the anterior aspect. The IOM consists of distal, middle, and proximal portions. The middle portion is a ligamentous complex (middle ligamentous complex) that is further divisible into the CB and the AB. Distal and proximal portions on either side of the middle portion comprise transparent membranous tissue (distal and proximal membranous portions) with holes for perforation of the interosseous artery. The DOB is present within the distal membranous portion. The proximal oblique cord is present on the anterior side of the forearm and the dorsal oblique accessory cord on the posterior side in the proximal membranous portion. R, radius; U, ulna.

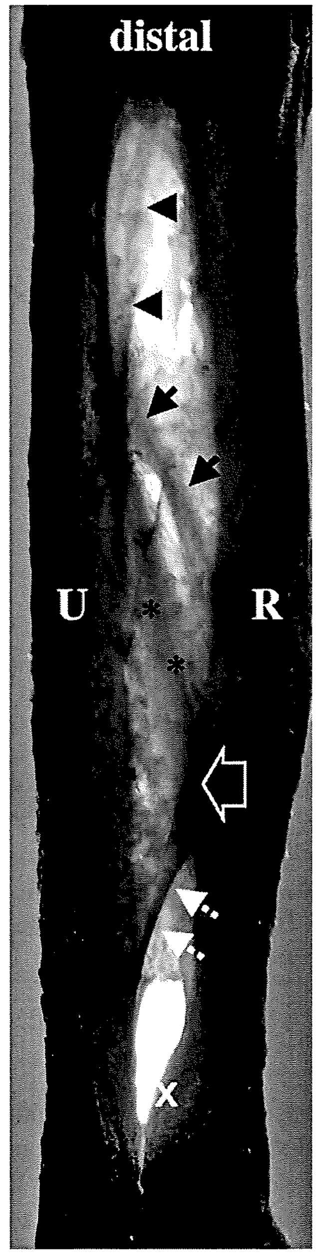

FIGURE 3: Backlit photograph of IOM ligaments. Asterisks indicate the CB as part of the middle ligamentous complex, which originates from the interosseous crest of the radius (white arrow), runs distally and ulnarly, and inserts into the interosseous border of the ulna. Arrows indicate the AB, which runs in a similar way to the CB. Arrowheads indicate the DOB within the distal membranous portion, which originates from around the distal one sixth of the ulnar shaft and inserts into the inferior rim of the sigmoid notch of the radius. Broken arrows indicate the dorsal oblique accessory cord on the posterior aspect of the forearm, which originates from around the distal two thirds of the ulnar shaft and inserts into the interosseous crest of the radius. The proximal oblique cord cannot be distinguished in this photograph because this cord is in contact with the surface of the radial tuberosity (x). R, radius; U, ulna.

crest of the radius, which is the interosseous ridge of the radius that projects most ulnaward, then coursed distally and ulnarly and inserted into the interosseous border of the ulna. The CB was seen in all specimens. The mean width was 9.7 ± 3 mm (range, 4.4–16 mm) measured perpendicular to its fibers, and the mean thickness was 1.3 ± 0.2 mm (range, 1–1.6 mm). The locations of the attachments of the CB on the radius and ulna are detailed in Table 1.

Accessory band: Several ligaments, which were in the same coronal plane as the CB, existed on either side of the CB in the middle ligamentous complex and were collectively termed the AB (see Figs. 2, 3). The fibers of the AB ran in almost the same direction as the CB

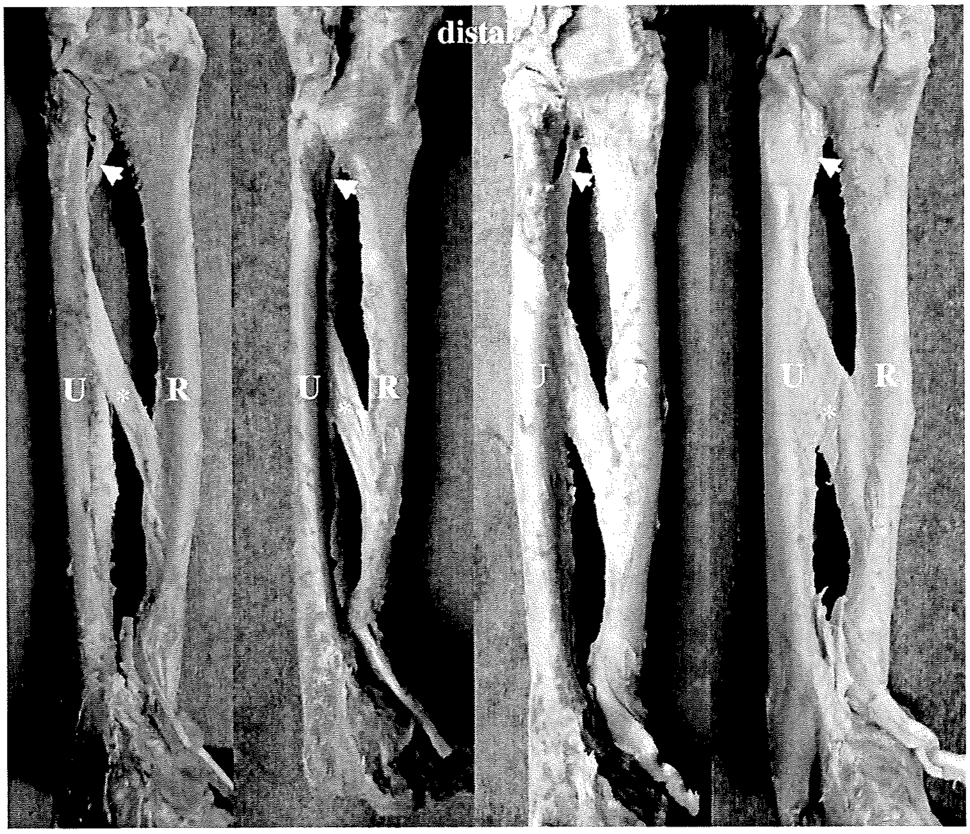

FIGURE 4: The CB and DOB, Four different right forearms are shown. Asterisks indicate the CB, and arrows indicate the DOB. The other ligamentous components were dissected. The CB is the thickest ligament and has a broad attachment. It originates from the interosseous crest of the radius, then courses distally and ulnarly and inserts into the interosseous border of the ulna. The CB was seen in all specimens.

fibers. The structure was less substantial (< 1 mm in thickness) and varied in location and number (Fig. 5). The AB was usually located distal to the CB, and the most distal ligament of the AB tended to be the stoutest of the AB fibers. In comparison, fibers were often absent proximal to the CB, and even if present, they were short and delicate. Of 30 specimens examined, the region distal to the CB showed a single ligament in 14 specimens, 2 ligaments in 3 specimens, 3 ligaments in 8 specimens, 4 ligaments in 1 specimen, 5 ligaments in 1 specimen, and 0 ligaments in 3 specimens. Conversely, the region proximal to the CB showed 0 ligaments in 17 specimens, 2 ligaments in 7 specimens, 3 ligaments in 5 specimens, and 4 ligaments in 1 specimen.

We chose the distal ligament for attachment measurement because it was the only structure of all AB fibers that existed in a relatively constant and stout fashion. The attachment locations of the AB fibers are detailed in Table 1.

Distal membranous portion

The distal membranous portion was on the distal side of the middle ligamentous complex, spanning between the radius and ulna under the region of the pronator quadratus muscle. A hole existed in that portion, through which the interosseous artery passed.

Distal oblique bundle: A relatively thick fiber ran within the distal membranous portion along the distal ulnar shaft in all specimens (see Figs. 2, 3). We named this bundle of fibers the distal oblique bundle (DOB). It existed in the same coronal plane as the CB and AB fibers. Although thickness varied widely among specimens, obvious fibers were seen in 12 of 30 specimens. The DOB originated from approximately the distal one-sixth area of the ulnar shaft, approximately coinciding with the proximal border of the pronator quadratus muscle, and ran distally toward the distal radioulnar joint (DRUJ; Fig. 6). The fibers blended into the capsular tissue of the DRUJ and eventually the DOB inserted to the inferior rim of the sigmoid notch of the

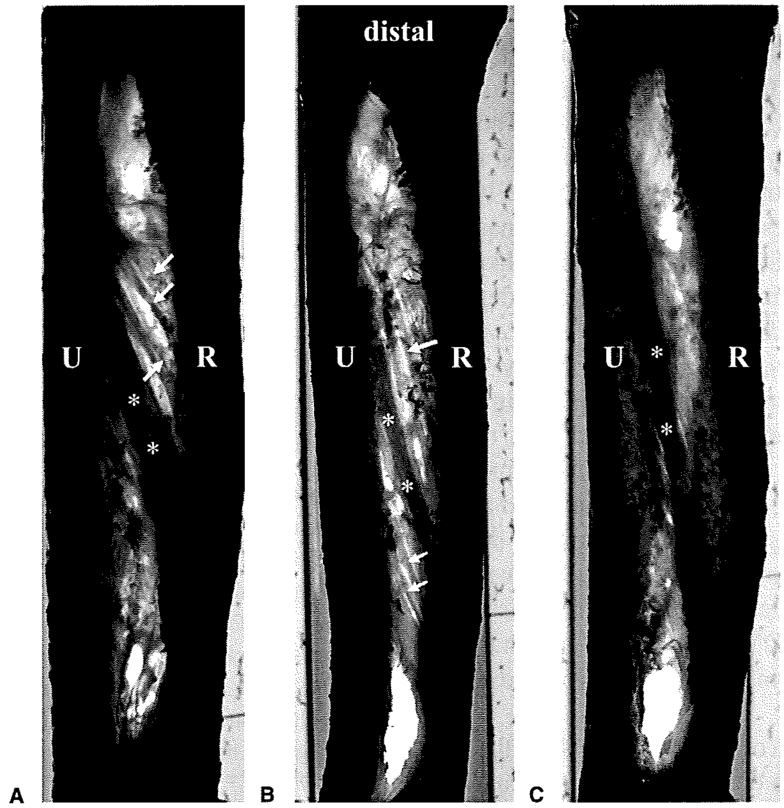

FIGURE 5: The AB. Three different right forearms are shown. Asterisks indicate the CB, and arrows indicate fibers of the AB. The fibers of the AB are less substantial than those of the CB. **A** Pattern of a few AB fibers distal to the CB, without any obvious fibers proximal to the CB. This pattern was seen often. **B** Pattern of AB fibers on either side of the CB. **C** Pattern with no obvious AB fibers on either side of the CB. R, radius; U, ulna.

radius. Furthermore, some fibers extended more distally along the anterior and posterior ridges of the sigmoid notch, so the DOB seemed to display continuity with the dorsal and palmar radioulnar ligaments of the triangular fibrocartilage complex (TFCC). The mean width was 4.4 ± 1.1 mm (range, 2–6 mm) and the mean thickness was 1.5 ± 0.5 mm (range, 0.5–2.6 mm).

The attachment locations of the DOB to the radius and ulna are listed in Table 1.

Proximal membranous portion

The proximal membranous portion was on the proximal side of the middle ligamentous complex. The proximal membranous portion was overlaid by the origin of the flexor digitorum profundus muscle on the anterior aspect of the forearm and by the supinator muscle on the posterior aspect. A hole existed in that portion, through which the interosseous artery passed.

Proximal oblique cord: A ligament called the proximal oblique cord or ligament of Weitbrecht[12,17] was seen in the most proximal interosseous space (Fig. 7; see also Fig. 2) in all specimens. The proximal oblique cord originated from the anterolateral aspect of the coronoid process of the ulna (ulnar tuberosity) and inserted just distal to the radial tuberosity. The proximal oblique cord lay on the surface of the biceps tendon that attaches to the radial tuberosity. The mean width was 3.7 ± 1.6 mm (range, 1.5–8 mm) and the mean thickness was 1.1 ± 0.5 mm (range, 0.4–2 mm).

The sites of attachment of the proximal oblique cord to the radius and ulna are listed in Table 1.

Dorsal oblique accessory cord: A ligament called the dorsal oblique accessory cord was seen on the posterior aspect of the forearm (Fig. 8; see also Figs. 2, 3), located under the origin of the abductor pollicis longus muscle. The dorsal oblique accessory cord was found in 16 of 30 specimens. This ligament originated from around the distal two thirds of the ulnar shaft and inserted into the interosseous crest of the radius. The mean width was 3.2 ± 1 mm (range, 1.9–5 mm), and the mean thickness was 0.9 ± 0.2 mm (range, 0.5–1 mm).

The sites of attachment of the dorsal oblique accessory cord to the radius and ulna are reported in Table 1.

DISCUSSION

Although past researchers have investigated the anatomy of the IOM,[1–7] to say that the history of IOM research is that of the CB is no exaggeration. The CB is frequently discussed in the literature because it is considered the most functional component of the IOM as the result of its stoutness and constancy. The name CB appears to have been first introduced by Hotchkiss and colleagues,[1] but the same formation was also described as the *intermediate descending fiber*[3]; the *cordlike portion*[4,6]; and the *tendinous part.*[5] Many cadaveric studies have been performed to investigate CB function.[1–3,8–11] They have revealed that the CB works as a restraint on the radius from proximal migration in cooperation with the radial head and the TFCC and also works as a load transmitter between the radius and ulna to redistribute load. Other studies[4,17–20] have indicated that the CB is an isometric component of the IOM and shows no change in tension during forearm rotation, thus providing stability to the forearm.

In comparison, the other components of the IOM have been described in only a few studies,[2–5] and their functions remain unclear. Skahen and colleagues[2] reported the AB and the proximal interosseous band, which corresponds to the dorsal oblique accessory cord in the present study. Poitevin[3] reported the proximal ascending bundle, which again corresponds to the dorsal oblique accessory cord in this study.

The functions of the AB have never been described in the literature. However, we suspect from the anatomical variations that function does not extend beyond a complementary nature, probably for the CB.

TABLE 1. Attachment Locations of Interosseous Membrane Ligaments

CB	
Radial origin (distal end)	53 ± 4% (46–61%)
Ulnar insertion (distal end)	29 ± 4% (24–36%)
Radial origin (proximal end)	64 ± 5% (51–74%)
Ulnar insertion (proximal end)	44 ± 5% (34–52%)
Distal ligament of the accessory band	
Radial origin	37 ± 5% (32–46%)
Ulnar insertion	23 ± 3% (19–26%)
DOB	
Ulnar origin	15 ± 2% (13–21%)
Radial insertion	9.9 ± 0.8% (8.3–11%)
Proximal oblique cord	
Ulnar origin	80 ± 2% (76–83%)
Radial insertion	79 ± 2% (75–84%)
Dorsal oblique accessory cord	
Ulnar origin	64 ± 9% (52–83%)
Radial insertion	62 ± 3% (56–68%)

Note: Based on 30 cadaveric forearms. Attachment locations are expressed as percentage of total bone length from the distal end. All data are represented as mean ± SD (range).

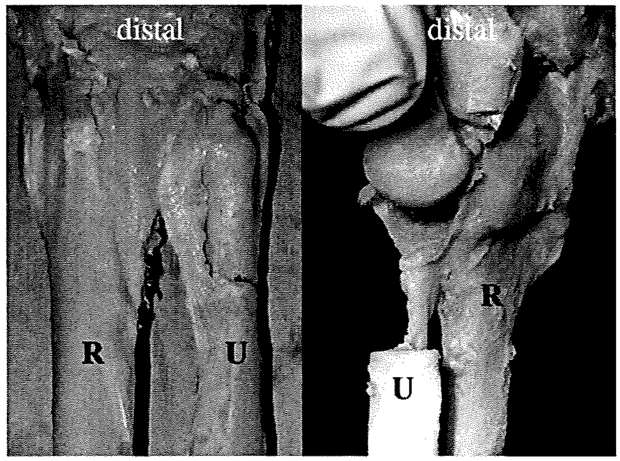

FIGURE 6: The DOB. The photograph on the left shows the DOB as seen from the dorsal aspect of the right forearm. This bundle originates from around the distal one sixth of the ulnar shaft and runs toward the DRUJ. The photograph on the right shows the DOB as seen from the ulnopalmar aspect of the same specimen. The ulna is cut just distal to the ulnar origin of the DOB and retracted distally. The DOB blends into the capsular tissue, through which it inserts into the inferior rim of the sigmoid notch of the radius. R, radius; U, ulna.

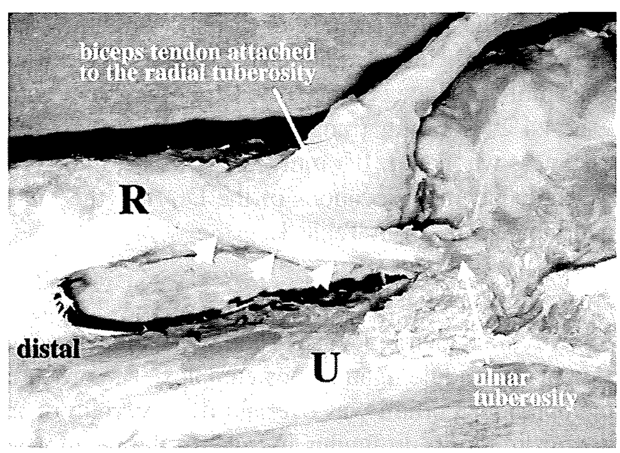

FIGURE 7: The proximal oblique cord. The right proximal forearm as seen from the anteromedial aspect. Arrows indicate the proximal oblique cord, originating from the anterolateral aspect of the coronoid process of the ulna (ulnar tuberosity) and inserting just distal to the radial tuberosity. The proximal oblique cord lies on the surface of the biceps tendon, which is attached to the radial tuberosity. R, radius; U, ulna.

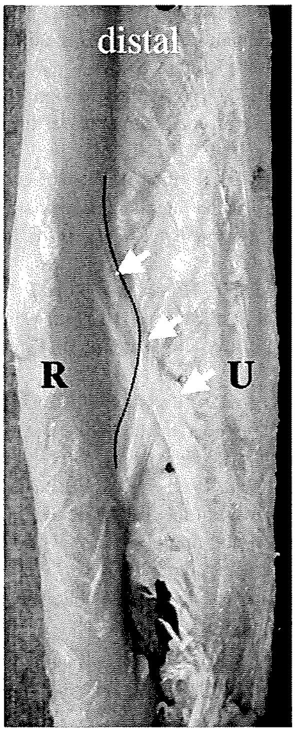

FIGURE 8: The dorsal oblique accessory cord. The right forearm viewed from the dorsal aspect. Arrows indicate the dorsal oblique accessory cord. The dorsal oblique accessory cord exists exclusively on the posterior aspect of the forearm, located under the region of origin of the abductor pollicis longus muscle. The cord originates from around the distal two thirds of the ulnar shaft and inserts into the interosseous crest of the radius (broken line). The dorsal oblique accessory cord was seen in 16 of 30 specimens. R, radius; U, ulna.

We identified the DOB, which was located within the distal membranous portion. Originating from around the distal one sixth of the ulnar shaft and running along the distal ulnar shaft toward the DRUJ, the DOB inserts into the inferior rim of the sigmoid notch of the radius. Furthermore, the DOB seems to exhibit continuity with the dorsal and palmar radioulnar ligaments of the TFCC. Watanabe and colleagues[21] insisted, in their biomechanical study, on the importance of the distal membranous portion of the IOM, which constrained volar and dorsal instability of the radius at the DRUJ in all forearm rotation positions. Kihara and colleagues[22] indicated that the distal membranous portion of the IOM acted as a secondary stabilizer of the DRUJ when the dorsal and palmar radioulnar ligaments of the TFCC were cut. Although we cannot know whether these researchers were aware of the structure of the DOB, we postulate from their studies that the anatomical relationship of the DOB to the TFCC suggests that the DOB functions to stabilize the DRUJ in cooperation with the TFCC because the DOB forms a ligament within the distal membranous portion. However, further biomechanical investigation is needed to confirm our hypothesis.

The proximal oblique cord is a relatively well-investigated component,[13–15,23] whereas descriptions of this ligament are variable. Some authors[23] have insisted that the structure is a remnant or accessory head of the flexor pollicis longus muscle (Gantzer's muscle), whereas another author[13] has stated that this cord represents a thickening of the fascia overlying the supinator muscle or perhaps even a degenerate part of the supinator muscle. We have also observed that the proximal oblique cord shows morphological variations to some extent, ranging from thick to relatively membranous. Conflicting descriptions of function have been reported.[13–15] Martin[13] and Tubbs and colleagues[14] described the cord as being most taut in supination and lax in both the neutral position and pronation in human cadavers, suggesting action as a restraint on excessive supination motions. Conversely, Patel[15] reported that the proximal oblique cord became most taut in pronation rather than in supination in the forelimbs of quadrupedal primates, suggesting a possible role in maintaining elbow stability when such primates stand on their pronated forelimbs. All of these authors concluded that the proximal oblique cord has little function in humans.

The present study clarified precise attachment locations of all representative IOM ligaments. This information will be useful in planning proper graft placement in ligament reconstruction surgery and in future biomechanical research into the function of the IOM ligaments.

REFERENCES

1. Hotchkiss RN, An K-N, Sowa DT, Basta S, Weiland AJ. An anatomic and mechanical study of the interosseous membrane of the forearm: pathomechanics of proximal migration of the radius. J Hand Surg 1989;14A:256–261.
2. Skahen JR III, Palmer AK, Werner FW, Fortino MD. The interosseous membrane of the forearm: anatomy and function. J Hand Surg 1997;22A:981–985.
3. Poitevin LA. Anatomy and biomechanics of the interosseous membrane: its importance in the longitudinal stability of the forearm. Hand Clin 2001;17:97–110.
4. Mori K. Experimental study on rotation of the forearm: functional anatomy of the interosseous membrane. J Jpn Orthop Assoc 1985; 59:611–622.
5. Nakamura T, Yabe Y, Horiuchi Y. Functional anatomy of the interosseous membrane of the forearm: dynamic changes during rotation. Hand Surg 1999;4:67–73.
6. Fujita M. An anatomical study on the interosseous membrane of the forearm. J Jpn Orthop Assoc 1995;69:938–950.
7. Schneiderman G, Meldrum RD, Bloebaum RD, Tarr R, Sarmiento A. The interosseous membrane of the forearm: structure and its role in Galeazzi fractures. J Trauma 1993;35:879–885.

8. Skahen JR III, Palmer AK, Werner FW, Fortino MD. Reconstruction of the interosseous membrane of the forearm in cadavers. J Hand Surg 1997A;22:986–994.
9. Rabinowitz RS, Light TR, Havey RM, Gourineni P, Patwardhan AG, Sartori MJ, et al. The role of the interosseous membrane and triangular fibrocartilage complex in forearm stability. J Hand Surg 1994A;19:385–393.
10. Birkbeck DP, Failla JM, Hoshaw J, Fyhrie DP, Schaffler M. The interosseous membrane affects load distribution in the forearm. J Hand Surg 1997;22A:975–980.
11. Pfaeffle HJ, Stabile KJ, Li ZM, Tomaino MM. Reconstruction of the interosseous ligament restores normal forearm compressive load transfer in cadavers. J Hand Surg 2005;30A:319–325.
12. Kapandji A. Biomechanics of pronation and supination of the forearm. Hand Clin 2001;17:111–122.
13. Martin BF. The oblique cord of the forearm. J Anat 1958;92:609–615.
14. Tubbs RS, O'Neil JT Jr, Key CD, Zarzour JG, Fulghum SB, Kim EJ, et al. Clin Anat 2007;20:411–415.
15. Patel BA. Form and function of the oblique cord *(chorda oblique)* in anthropoid primates. Primates 2005;46:47–57.
16. Chandler JW, Stabile KJ, Pfaeffle HJ, Li ZM, Woo SL-Y, Tomaino MM. Anatomic parameters for planning of interosseous ligament reconstruction using computer-assisted techniques. J Hand Surg 2003;28A:111–116.
17. Hollister AM, Gellman H, Waters RL. The relationship of the interosseous membrane to the axis of rotation of the forearm. Clin Orthop Relat Res 1994;298:272–276.
18. Nakamura T, Yabe Y, Horiuchi Y. In vivo MR studies of dynamic changes in the interosseous membrane of the forearm during rotation. J Hand Surg 1999;24B:245–248.
19. Nakamura T, Yabe Y, Horiuchi Y, Yamazaki N. Three-dimensional magnetic imaging of the interosseous membrane of forearm: a new method using fuzzy reasoning. Magn Reson Imaging 1999;17:463–470.
20. Nakamura T, Yabe Y, Horiuchi Y, Seki T, Yamazaki N. Normal kinematics of the interosseous membrane during forearm pronation-supination: a three-dimensional MRI study. Hand Surg 2000; 5:1–10.
21. Watanabe H, Berger RA, Berglund LJ, Zobitz ME, An KN. Contribution of the interosseous membrane to distal radioulnar joint constraint. J Hand Surg 2005;30A:1164–1171.
22. Kihara H, Short WH, Werner FW, Fortino MD, Palmer AK. The stabilizing mechanism of the distal radioulnar joint during pronation and supination. J Hand Surg 1995;20A:930–936.
23. Forster A. Uber den morphologischen Wert der Chorda oblique antebrachii anterior und der Chorda oblique antebrachii posterior. Z Morphol Anthropol 1905;8:62–79.